An Amphipathic Helix Directs Cellular Membrane Curvature Sensing and Function of the BAR Domain Protein PICK1

Herlo, Rasmus; Lund, Viktor K.; Lycas, Matthew D.; Jansen, Anna M.; Khelashvili, George; Andersen, Rita Chan; Bhatia, Vikram; Pedersen, Thomas S.; Albornoz, Pedro B. C.; Johner, Niklaus; Ammendrup-Johnsen, Ina; Christensen, Nikolaj R.; Erlendsson, Simon; Stoklund, Mikkel; Larsen, Jannik B.; Weinstein, Harel; Kjærulff, Ole; Stamou, Dimitrios; Gether, Ulrik; Madsen, Kenneth Lindegaard

Published in:
Cell Reports

DOI:
10.1016/j.celrep.2018.04.074

Publication date:
2018

Document version
Publisher's PDF, also known as Version of record

Article

Cell Reports

An Amphipathic Helix Directs Cellular Membrane Curvature Sensing and Function of the BAR Domain Protein PICK1

Graphical Abstract

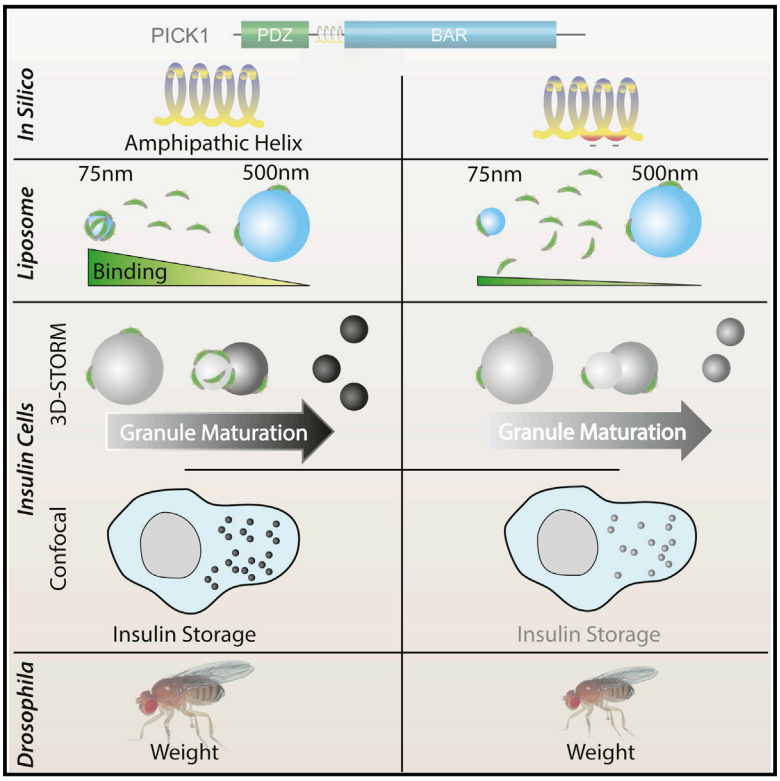

Highlights

- ICA69, PICK1, and arfaptins have an amphipathic helix N-terminal to their BAR domains
- The amphipathic helix directs curvature-sensitive binding of PICK1 to insulin granules
- Disruption of the amphipathic helix compromises insulin storage and growth

Authors

Rasmus Herlo, Viktor K. Lund, Matthew D. Lycas, ..., Dimitrios Stamou, Ulrik Gether, Kenneth L. Madsen

Correspondence

gether@sund.ku.dk (U.G.), kennethma@sund.ku.dk (K.L.M.)

In Brief

Herlo et al. identify amphipathic helices N-terminal to BAR domains in ICA69, PICK1, and arfaptins, which direct curvature-sensitive binding to liposomes and insulin granules during maturation. Disruption of this motif reduces membrane binding to curved, but not flat, membranes, leading to compromised insulin storage and growth deficiency in flies.

Herlo et al., 2018, Cell Reports *23*, 2056–2069
May 15, 2018
https://doi.org/10.1016/j.celrep.2018.04.074

CellPress

OPEN ACCESS
CellPress

Cell Reports
Article

An Amphipathic Helix Directs Cellular Membrane Curvature Sensing and Function of the BAR Domain Protein PICK1

Rasmus Herlo,[1] Viktor K. Lund,[1] Matthew D. Lycas,[1] Anna M. Jansen,[1] George Khelashvili,[3] Rita C. Andersen,[1] Vikram Bhatia,[2] Thomas S. Pedersen,[1] Pedro B.C. Albornoz,[3] Niklaus Johner,[3] Ina Ammendrup-Johnsen,[1] Nikolaj R. Christensen,[1] Simon Erlendsson,[1] Mikkel Stoklund,[1] Jannik B. Larsen,[2] Harel Weinstein,[3] Ole Kjærulff,[1] Dimitrios Stamou,[2] Ulrik Gether,[1,*] and Kenneth L. Madsen[1,4,*]

[1]Molecular Neuropharmacology and Genetics Laboratory, Lundbeck Foundation Center for Biomembranes in Nanomedicine, Department of Neuroscience, Faculty of Health and Medical Sciences, The Panum Institute - Mærsk Tower, University of Copenhagen, 2200 Copenhagen N, Denmark

[2]Bionanotechnology and Nanomedicine Laboratory, Lundbeck Foundation Center for Biomembranes in Nanomedicine, Department of Chemistry, and Nano-Science Center, University of Copenhagen, 2300 Copenhagen Ø, Denmark

[3]Department of Physiology and Biophysics, Weill Cornell Medical College, Cornell University, 1300 York Avenue, New York City, NY 10065, USA

[4]Lead Contact

*Correspondence: gether@sund.ku.dk (U.G.), kennethma@sund.ku.dk (K.L.M.)

https://doi.org/10.1016/j.celrep.2018.04.074

SUMMARY

BAR domains are dimeric protein modules that sense, induce, and stabilize lipid membrane curvature. Here, we show that membrane curvature sensing (MCS) directs cellular localization and function of the BAR domain protein PICK1. In PICK1, and the homologous proteins ICA69 and arfaptin2, we identify an amphipathic helix N-terminal to the BAR domain that mediates MCS. Mutational disruption of the helix in PICK1 impaired MCS without affecting membrane binding per se. In insulin-producing INS-1E cells, super-resolution microscopy revealed that disruption of the helix selectively compromised PICK1 density on insulin granules of high curvature during their maturation. This was accompanied by reduced hormone storage in the INS-1E cells. In *Drosophila*, disruption of the helix compromised growth regulation. By demonstrating size-dependent binding on insulin granules, our finding highlights the function of MCS for BAR domain proteins in a biological context distinct from their function, e.g., at the plasma membrane during endocytosis.

INTRODUCTION

Many cellular processes involve transient association of cytosolic proteins with lipid membranes. Some membrane-associated proteins are directed to biochemically distinct membranes by domains that recognize specific phosphoinositides (PIPs), such as PH (pleckstrin homology) domains (Moravcevic et al., 2012). Others localize to biophysically distinct membranes that are highly curved, by partially inserting hydrophobic/lipidated residues or amphipathic helices (AHs) in the cytosolic leaflet (Gallop and McMahon, 2005; Hatzakis et al., 2009; Iversen et al., 2015; Larsen et al., 2015; Madsen et al., 2010). As an interesting consequence, membrane curvature may be important for organizing cellular processes within biochemically identical compartments, and AHs in numerous proteins are functionally important in processes as diverse as endoplasmic reticulum (ER)-Golgi transport, autophagy and endocytosis (Doherty and McMahon, 2009; Drin and Antonny, 2010; Nguyen et al., 2017).

N-BAR (Bin/Amphiphysin/Rvs) domains constitute a particular class of membrane binding and deforming domains. They function as homodimeric/heterodimeric crescent-shaped assemblies flanked by AHs and are found in proteins, such as endophilins and amphiphysins, that serve in cellular functions involving membrane reorganization (Gallop and McMahon, 2005). The domains show semi-specific lipid binding based on electrostatics while simultaneously displaying membrane-curvature-sensitive binding (Peter et al., 2004). On spherical membranes, membrane curvature sensing (MCS) depends on hydrophobic insertion of the N-terminal AHs (Bhatia et al., 2009; Cui et al., 2011). On membrane tubes, MCS likely relies on the BAR domain itself (Sorre et al., 2012; Wu and Baumgart, 2014), which, in addition, can tubulate membranes (Mim et al., 2012).

In cells, N-BAR domain proteins are generally localized to high-curvature membranes (Farsad et al., 2001; Peter et al., 2004). However, it is difficult to separate, both functionally and mechanistically, the relative contributions to this localization coming from MCS versus induced deformation. Recent studies have addressed the recruitment to high-curvature membranes induced by external membrane deformation, but the biological implications remain unclear (Galic et al., 2012; Hsieh et al., 2012). Indeed, probing the biological implications of MCS for N-BAR proteins has proven challenging, due to the lack of mutations that impair MCS without affecting membrane binding per se.

ICA69 (Islet Cell Autoantigen 69 kDa), ICA69-L (Islet Cell Autoantigen 69 kDa-like), PICK1 (Protein Interacting with C Kinase),

and arfaptins 1 and 2 constitute another subgroup of BAR domain proteins (hereinafter termed IPA BARs) that is evolutionary closely related to the N-BAR domains (Peter et al., 2004). Recent studies have suggested a common role of these proteins in secretory vesicle biogenesis in endocrine cells (Cao et al., 2013; Cruz-Garcia et al., 2013; Gehart et al., 2012; Holst et al., 2013; Jansen et al., 2009). PICK1 also plays a key role in regulating surface expression of, e.g., AMPA-type glutamate receptors (AMPARs) in the brain (Hanley, 2008; Xu and Xia, 2006-2007). Importantly, the PICK1 BAR domain can bind membranes (Jin et al., 2006; Lu and Ziff, 2005; Madsen et al., 2008) and the arfaptin 2 BAR domain both binds and tubulates liposomes (Peter et al., 2004). It is unknown, however, whether IPA BARs operate mechanistically like N-BARs and how putative MCS may shape their function.

Here, we show that an N-terminal AH precedes the BAR domain in the IPA BAR protein family in a manner similar to what is seen for classical N-BAR domains. We also demonstrate that the IPA proteins, indeed, bind membranes in a curvature-sensitive manner and that their MCS capacity is recapitulated by the helix alone. Importantly, mutational disruption of the AH in PICK1 compromises MCS *in vitro* without affecting membrane binding of PICK1 per se. Consistent with impaired MCS, we show by molecular replacement that mutation of the helix reduces selective recruitment of PICK1 to insulin-containing granules. Moreover, we find that the decreased recruitment is accompanied by reduced hormone storage in insulin-producing INS-1E cells. Also, we provide evidence for a role of the helix *in vivo* by substantiating its importance for growth regulation in *Drosophila*. Altogether, our data demonstrate that IPA BARs are N-BARs and suggest that the N-terminal AH governs cellular MCS and is critical for the physiological role of PICK1 in endocrine cells. Moreover, by demonstrating that MCS can direct the localization and function of a BAR domain protein on preformed vesicular structures, our findings distinguish MCS from deformation, two processes that are difficult to separate during, e.g., endocytosis.

RESULTS

IPA BAR Proteins Display Curvature-Sensitive Membrane Binding

To probe the interaction of IPA BAR domain proteins with curved spherical membranes resembling vesicular carriers in, e.g., regulated secretion, we used a single-liposome curvature (SLiC) assay (Bhatia et al., 2009; Hatzakis et al., 2009; Larsen et al., 2015). We used stochastic optical reconstruction microscopy (STORM) to substantiate uniform incorporation of the membrane dye DiD across liposomes sizes tethered on a glass surface (Figure S1), thereby validating the DiD signal as a reliable measure of liposome size/curvature. After incubation with fluorescently labeled protein, we detected bound protein (protein channel) on single immobilized liposomes (vesicle channel) by confocal microscopy (Figure 1A). Fluorescently labeled PICK1 co-localized completely with the liposome signal, indicating strong membrane binding (Figure 1A). However, as previously observed for liposome binding by insertion-based mechanisms (Bhatia et al., 2009), PICK1 bound to only ~50% of the liposomes (Figures 1A and 1B). Likewise, arfaptin 2 and ICA69 demonstrated fractional binding (Figure 1B). In comparison, the N-BAR protein endophilin bound only ~10% of the vesicles (Bhatia et al., 2009).

The membrane signal from diffraction-limited vesicles was converted to absolute diameter using an extensively tested calibration procedure (see Experimental Procedures), enabling us to plot the protein density as a function of liposome size. We observed the liposome binding of the BAR proteins to be highly membrane curvature sensitive, exhibiting a 25- to 30-fold increase in protein density on small (75-nm), over large (500-nm), liposomes (Figures 1C–1E). In order to compare quantitatively the MCS ability for the three proteins, we derived the exponent α from a power law fit of the density as function of radius r (Hatzakis et al., 2009). Indeed, a power law fitted the data well (Figure 1F), and all three proteins demonstrated stronger MCS than endophilin N-BAR (dashed line) (Figure 1G) (Bhatia et al., 2009; Hatzakis et al., 2009). We also performed concentration-dependent binding curves, demonstrating that, although the absolute density for large (500-nm) liposomes was lower than for small (75-nm) liposomes (note different y axis), the concentration dependency appeared almost identical (Figure 1H). This is in agreement with previous findings and suggests that curvature sensing is not governed by different affinities for large versus small liposomes but rather by available binding sites (Bhatia et al., 2009; Hatzakis et al., 2009). For ICA69, we found an apparent monophasic curve showing an estimated affinity < 1 μM, similar to what we previously observed for endophilin (Bhatia et al., 2009). For PICK1, we observed a biphasic binding curve that was also upward shifted, which implies two separate membrane-binding motifs. The arfaptin2 binding curve did not reach saturation, indicating lower affinity of this protein (Figure 1H). Of note, the absolute binding densities correlated overall well with fractional binding (Figure 1B).

Identification of Amphipathic Helices N-Terminal to the BAR Domains in IPA BAR Proteins

The BAR domains of the IPA BAR proteins are closely related evolutionarily to other N-BAR domains (Figure 2A). In ICA69, the BAR domain is localized to the N terminus, like in endophilins and amphiphysins, and the C-terminal part of the protein (ICAC) is unstructured (Figures 2B and S2). In PICK1, the BAR domain is preceded by a PDZ domain, and in the arfaptins, the BAR domain is preceded by ~100 residues, which, according to a nuclear magnetic resonance (NMR) analysis are unstructured (Figures 2B and S3). Interestingly, helical wheel projections of the three sequences preceding the BAR domains suggested strong amphipathic properties, and the isolated putative helices fused to glutathione S-transferase (GST) recapitulated the curvature-sensitive liposome binding observed for the full-length proteins (Figures 2C–2E). In addition, circular dichroism (CD) spectroscopy on peptides corresponding to the predicted N-terminal AHs confirmed liposome-induced α-helix formation (Figures 2F–2H). Together, these data support the conclusion that the BAR domains in the IPA family are preceded by AHs, like in the classical N-BAR domains, as recently suggested for PICK1 and arfaptins (Cruz-Garcia et al., 2013; Holst et al., 2013; Jin et al., 2006) and that these AHs are sufficient to mediate the curvature-sensitive membrane binding observed for the IPA BAR proteins.

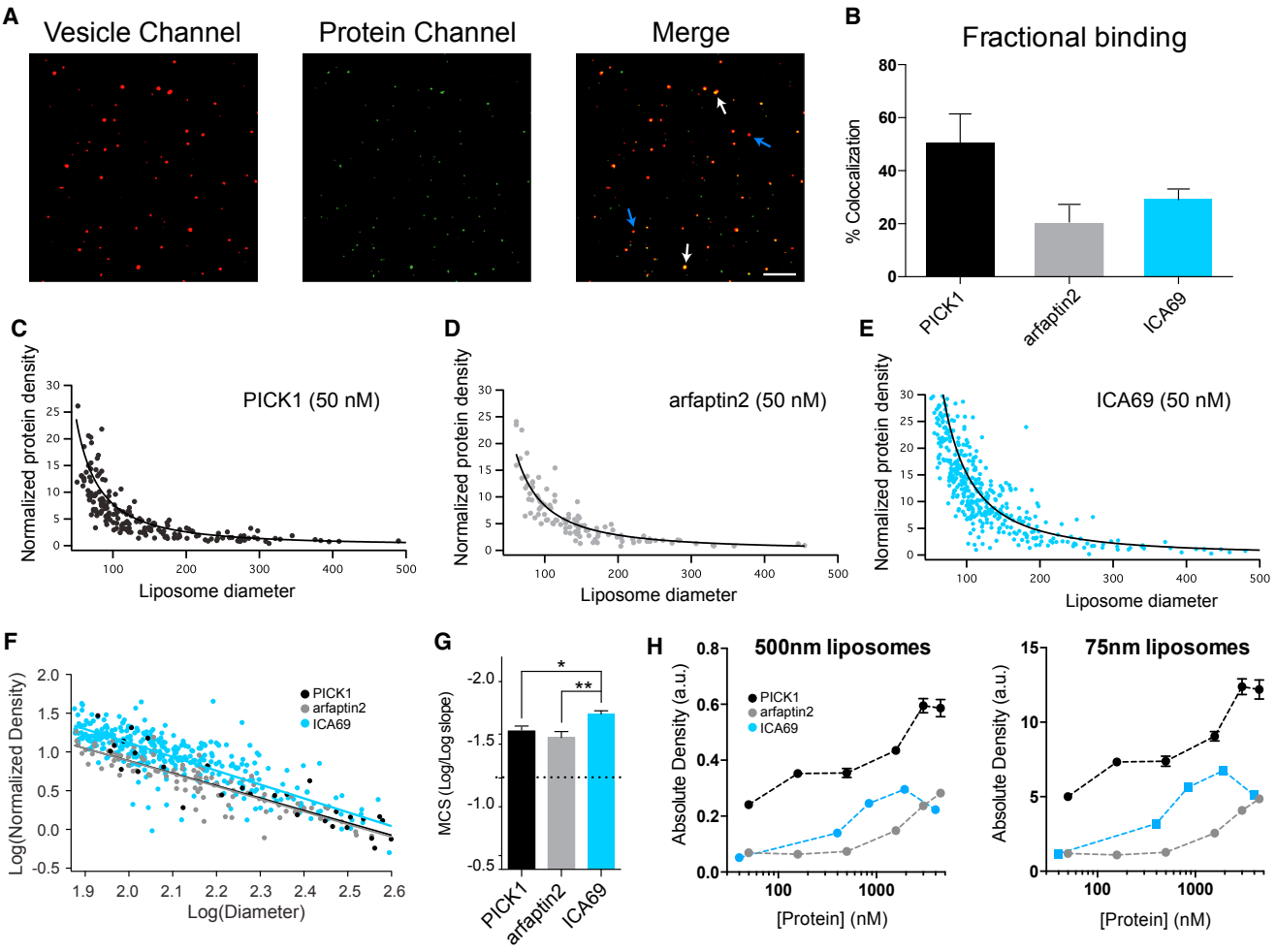

Figure 1. Fractional and Membrane Curvature-Sensitive Liposome Binding of the IPA BAR Domain Proteins

Purified and fluorescently labeled PICK1, ICA69, and arfaptin 2 were analyzed in the SLiC assay (Hatzakis et al., 2009) to assess spherical liposome binding properties.

(A) Representative confocal micrographs of surface-tethered fluorescently labeled liposomes (DiD) after incubation with 50 nM Alexa-488-conjugated PICK1. Left: vesicle channel; middle: protein channel; right: merged image. White arrows: protein-bound liposomes. Blue arrows: liposomes with no protein bound. Scale bar, 5 μm.

(B) Quantification of the fractional liposome binding for fluorescently labeled PICK1, arfaptin 2, and ICA69 (50 nM) (percent colocalization and, thus, fraction of liposomes with bound protein). Data indicate means ± SEM, n = 3.

(C–E) Representative graphs showing binding (normalized protein density) protein to liposomes of different diameters for (C) PICK1, (D) arfaptin 2, and (E) ICA69 (50 nM). Each dot represents a single vesicle.

(F) Log-log representation of the data described above. The linear relationship on the log-log plot indicates an insertion-based binding mechanism, with the slope reflecting the degree of curvature sensing (MCS).

(G) Quantification of curvature sensing (slopes from log-log plots in F) demonstrating high curvature sensing for all three proteins. Data indicate means ± SEM; n = 3. *p < 0.05; **p < 0.01, one-way ANOVA, Tukey's multiple comparisons test).

(H) Representative curves of concentration-dependent liposome absolute binding for PICK1, arfaptin 2, and ICA69 corrected for labeling efficiency: PICK1, 37%; arfaptin 2, 85%; and ICA69, 165% for sizes 500 nm (left) and 75 nm (right). Points were extracted from experiments similar to those in (C)–(E) but at 6 different concentrations and represent the fitted value ± SEM from (C)–(E) (full line) at 500 and 75 nm.

To investigate the mode of helix insertion into the membrane, we carried out molecular dynamics (MD) simulations in a protocol starting with coarse-grained (CG) simulations using the Martini force field (Marrink et al., 2007; Monticelli et al., 2008) and continued for detailed refinement with all-atom (AA) unbiased simulations using Groningen Machine for Chemical Simulations (Gromacs) (Hess et al., 2008). The results were used to quantify the level of insertion of the PICK1, arfaptin 2, and ICA69 putative AHs into dioleoylphosphatidylethanolamine (DOPE)/dioleoylphosphatidylcholine (DOPC)/PIP_2 membranes. Figures 2I–2K (top) shows average insertion depths for the three peptides, and Figures 2I–2K (bottom) depicts final snapshots (after 8 μs). A well-defined stretch of residues in PICK1, flanked by L114 and M129, was found to strongly penetrate the membrane in

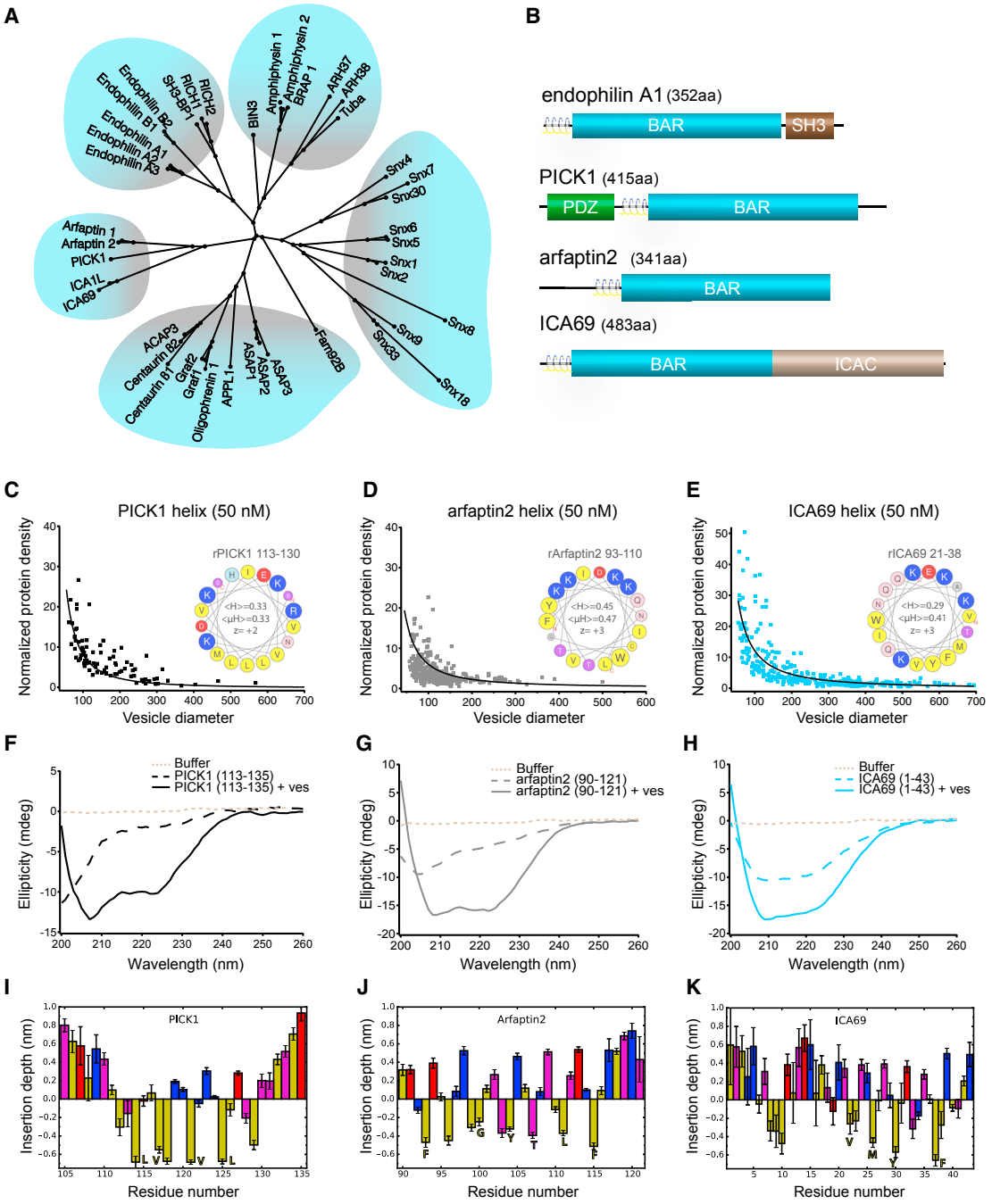

Figure 2. Amphipathic Helices N-Terminal to the BAR Domains in the IPA BARs Mediate Curvature-Sensitive Membrane Binding

(A) Phylogenetic tree of proteins belonging to the BAR-domain family.

(B) Domain organization and position of AHs (blue/yellow) N-terminal to the BAR domains in endophilin A1, PICK1, arfaptin 2, and ICA69.

(C–E) Representative graphs showing SLiC of the putative AHs (fused to GST) from (C) PICK1 (105–135), (D) arfaptin 2 (90–121), and (E) ICA69 (1–43) at a 50 nM concentration. Each dot represents a single liposome. Inserts: helical wheel projections (Gautier et al., 2008) of putative PICK1, arfaptin 2, and ICA69 AHs. < H > indicates hydrophobicity; < μH > indicates hydrophobic moment; z indicates total charge.

(F–H) Representative CD spectra on peptides corresponding to the AHs in (F) PICK1 (amino acids [aa] 113–135), (G) arfaptin 2 (aa 90–121), and (H) ICA69 (aa 1–43). In all cases, liposomes increase helical content. ves, vesicles.

(I–K) Top: insertion depths from CG molecular dynamics simulations into a DOPE/DOPC/PIP_2 membrane measured for each residue of (I) PICK1 (aa 105–135), (J) arfaptin 2 (aa 90–121), and (K) ICA69 (aa 1–43) peptides. Colors: yellow indicates hydrophobic; magenta indicates polar; blue indicates positive; and red indicates negative. Error bars indicate means ± SEM.

See also Figures S1, S2, and S3.

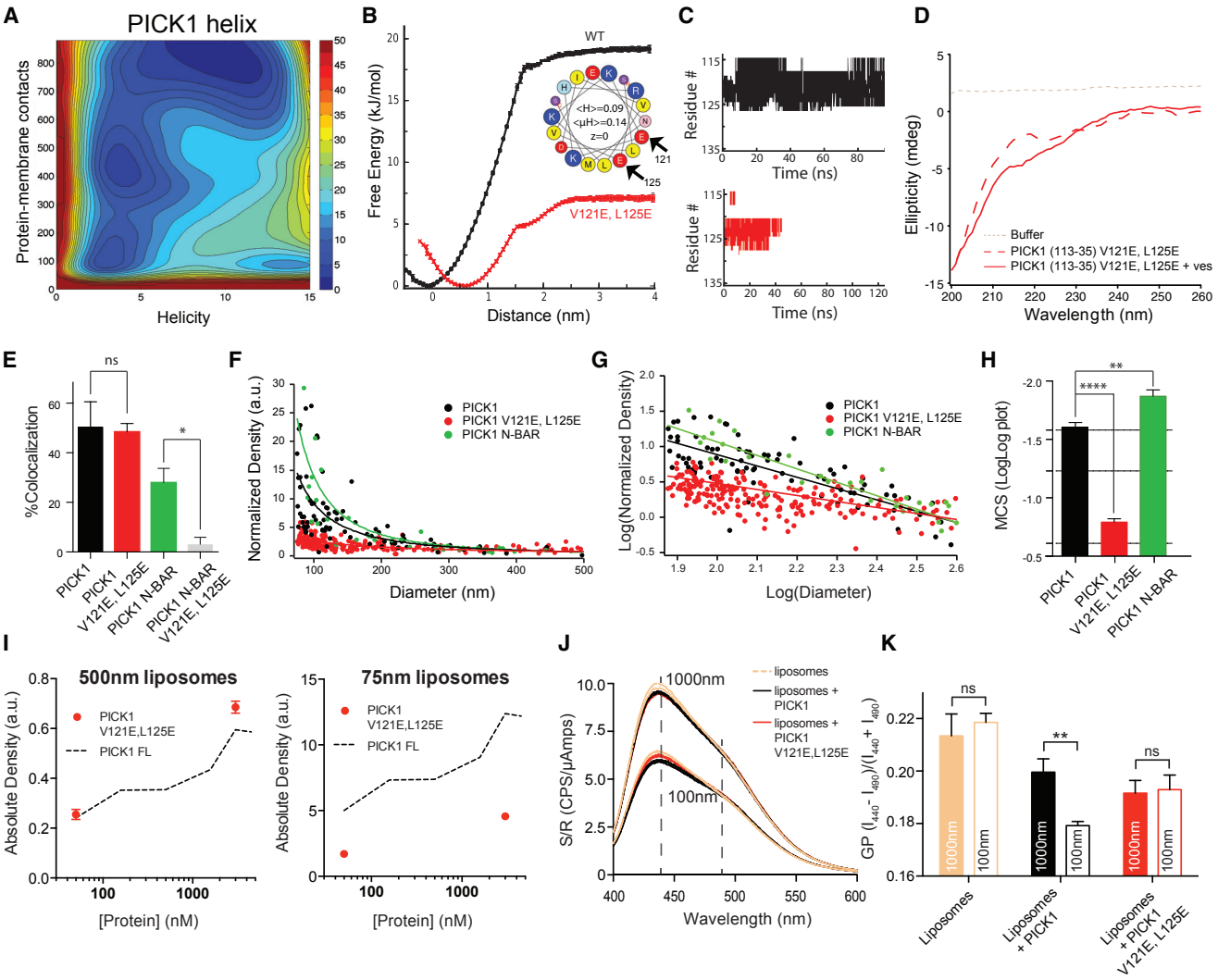

Figure 3. Disruption of the AH Compromises MCS without Affecting Overall Liposome Binding of PICK1

(A) Free energy landscape for the folding of the PICK1 AH peptide and its binding to the membrane. Membrane binding is quantified through protein-membrane contacts, and folding into a helix is expressed by a helicity parameter RMSD (see Supplemental Experimental Procedures). A free energy minimum (dark blue contours) was found for the conformations in which PICK1 peptide was membrane bound (high protein-membrane contact count) and in a helical state (large values of the helicity parameter).

(B) Free energy of binding of the PICK1 WT (black) and PICK1 V121E, L125E peptide (red) (helical wheel prediction of the mutant is shown in insert) to a DOPE/DOPC/PIP_2 lipid membrane obtained from CG-MD simulations. Errors were estimated using Monte Carlo bootstrapping (see Figure S4, top panel).

(C) Time-course of the secondary structure of the PICK1 WT (black) and the PICK1 V121E, L125E (red) peptides during the course of the AA MD simulations (the y axis indicates helical conformation for a particular residue).

(D) CD spectra on peptide corresponding to the AH in PICK1 (113–135) with V121E and L125E. No helical structure is induced in the mutant peptide in the presence of liposomes.

(E) Quantification of the fractional binding in the liposome-binding assay for PICK1 (same as in Figure 1B); PICK1 V121E, L125E; PICK1 N-BAR; and PICK1 N-BAR V121E, L125E at a 50-nM concentration. Error bars indicate means ± SEM; n = 3. *p < 0.05, unpaired t test; ns, not significant.

(F) Representative graph (of n = 3) showing binding of fluorescently (Alexa 488) labeled protein (normalized protein density) to immobilized liposomes of different diameters for PICK1 WT; PICK1 V121E, L125E; and PICK1 N-BAR (50 nM). Each dot represents a single vesicle. The data were fitted to a power-law function.

(G) Log-log representation of the data from (E) yielding linear representation of the power-law fits of WT and mutants, with the slope giving the MCS.

(H) Quantification of MCS (slope from log-log plots in F) (means ± SEM, n = 3; **p < 0.01; ****p < 0.0001, one-way ANOVA, Dunnett's multiple comparisons test), showing improved MCS upon deletion of the PDZ domain (PICK1 N-BAR) and abolished MCS for PICK1 BAR V121E, L125E.

(I) Representative curves of concentration-dependent liposome binding of PICK1 V121E, L125E corrected for labeling efficiency (PICK1 V121E, L125E, 19%) for sizes 500 nm (left) and 75 nm (right) (compared to WT from Figure 1, as dashed lines). Points (red) were extracted from experiments similar to those indicated in (F) at high (3-μM) and low (40-nM) concentrations and represent the fitted value ± SEM from (F) (full line) at 500 and 75 nm, respectively.

(legend continued on next page)

these simulations, and four hydrophobic residues, L114, L118, V121, and L125, inserted the deepest into the bilayer core.

To determine the free energy landscape for binding to the membrane (quantified through protein-membrane contacts), and folding into a helix (expressed by a helicity parameter root-mean-square deviation [RMSD]), we used AA MD simulations, together with the Unified Free Energy Dynamics (UFED) biasing scheme (Chen et al., 2012), as described in the Supplemental Experimental Procedures. As shown in Figure 3A, a free energy minimum (dark blue contours) was found for the conformations in which the PICK1 peptide was both membrane bound (high protein-membrane contact count) and in a helical state (large values of the helicity parameter). In contrast, unfolded conformations (small helicity values) are seen to be more favorable in solution. This is in agreement with the CD experiments and supports that the peptide likely is disordered in solution but adopts a helical conformation when membrane bound.

The role of the amphipathic nature of the PICK1 helix in achieving structured binding to the membrane and MCS was probed by introducing two negative charges at positions 121 and 125 (V121E, L125E) (see Figures 3B and S4, top panel). Enhanced umbrella sampling protocols and CG MD simulations showed that the calculated free energy of binding for PICK1 V121E, L125E was only half that of PICK1 wild-type (WT) (Figure 3B. AA MD simulations further showed that, whereas WT peptide maintained a stable helical structure at the membrane surface (Figure 3C, black), the V121E, L125E peptide became unstructured after ~50 ns of simulations (Figure 3C, red), suggesting that it is preferentially disordered, even if it is initially a helix when bound to the membrane. The predictions from the computational study were tested and validated experimentally with CD spectroscopy, showing that, unlike the WT peptide, the CD spectrum of the V121E, L125E construct was unchanged upon vesicle addition (Figure 3D).

The AH Is Critical for Spherical Curvature Sensing but Not for Fractional Membrane Binding of PICK1

To characterize further the effects of the mutations, we purified full-length PICK1 (V121E, L125E). The integrity of the primary and tertiary structure of PICK1 V121E, L125E was confirmed both by mass spectrometry and small-angle X-ray scattering, which also demonstrated unaltered oligomerization propensity in solution (Figures S5A and S5B). PDZ domain binding was, likewise, similar to that of PICK1 WT (Figure S5C). In the SLiC assay, we surprisingly observed that the fractional binding of PICK1 V121E, L125E (50 nM) to liposomes was similar to that of WT (Figure 3E), in contrast to our previous findings for endophilin, in which a single mutation in the AH (F10E) essentially eliminated fractional binding (Bhatia et al., 2009). This suggested that additional motifs are involved in PICK1 liposome binding and, indeed, that the PICK1 PDZ domain was previously shown to bind membranes (Pan et al., 2007). Therefore, we measured membrane binding of the PICK1 N-BAR domain without the PDZ domain (PICK1 101-416), which showed a non-significant reduction in the fractional binding (Figure 3E). However, introducing the V121E, L125E mutation in this (PICK1 101-416) construct (PICK1 N-BAR V121E, L125E) nearly abolished fractional binding (Figure 3E), analogous to our previous findings for endophilin (Bhatia et al., 2009). Together, these data suggest that the AH and the PDZ domain jointly determine membrane binding of PICK1.

Although fractional binding of PICK1 V121E, L125E did not change, its MCS capacity was dramatically reduced, as we observed little increase in protein density on small liposomes compared to the large ones (Figures 3F–3H). Conversion to absolute densities of bound mutant protein showed uncompromised binding to large (500-nm) liposomes, both at low (50-nM) and high (3-μM) concentrations of protein, whereas binding to small (75-nm) liposomes was severely compromised at both concentrations, further underscoring that MCS is largely independent on protein concentration (Figure 3I).

To assess whether the helix inserts into the membrane also in the context of the full-length protein, and that this insertion is impaired by the mutation, we utilized an approach used recently to show that the ability of endophilin to quench the lipophilic fluorescent dye 6-dodecanoyl-2-dimethylaminonaphthalene (laurdan) relied on membrane insertion of the amphipathic H0 and H1 helices, but not on protein association to the membrane as such (Poudel et al., 2016). We tested the ability of PICK1 WT and V121E, L125E to quench laurdan fluorescence using generalized polarization (GP) as a measure. GP for small (extruded through a 100-nm filter) and large (extruded through a 1,000-nm filter) liposomes did not differ (although the overall fluorescence intensity was lower for small compared to large liposomes) (Figures 3J and 3K). Also, incubation of the liposomes with either WT or mutant reduced GP of laurdan in the large liposomes to the same extent, possibly as a result of the PDZ domain insertion. However, only PICK1 WT, and not the mutant, further reduced GP for laurdan in the small liposomes (Figures 3J and 3K). This supports the conclusion that, in the context of the full-length protein, the WT helix——and, only to a lesser degree, the mutant helix—is likely to insert into the membrane.

The AH Encodes Curvature-Sensitive Cellular Localization of PICK1 in Insulin-Secreting INS-1E Cells

PICK1 displays punctate localization to Golgi-proximal structures in secretory cells, including insulin-producing INS-1E (Cao et al., 2013; Holst et al., 2013). We surmised that this would make it possible to assess putative MCS in these cells. We used a molecular replacement strategy to substitute endogenous PICK1, using short hairpin RNA (shRNA)-mediated knockdown, with simultaneous expression of shRNA-resistant GFP-PICK1 (Citri et al., 2010). Similar to our previous findings in growth hormone-producing GH1 cells (Holst et al., 2013), the punctate

(J) Representative curves showing PICK1- and PICK1 V121E, L125E-dependent quenching of laurdan (dashed line at 440 nm) in 1,000- and 100-nm liposomes. (K) Quantification of GP = $(I_{440}–I_{490})/(I_{440}–I_{490})$ from curves in I. Error bars indicate means ± SEM; n = 3. **p < 0.01, two-way ANOVA, Bonferroni post-test; ns, not significant.
See also Figures S4 and S5.

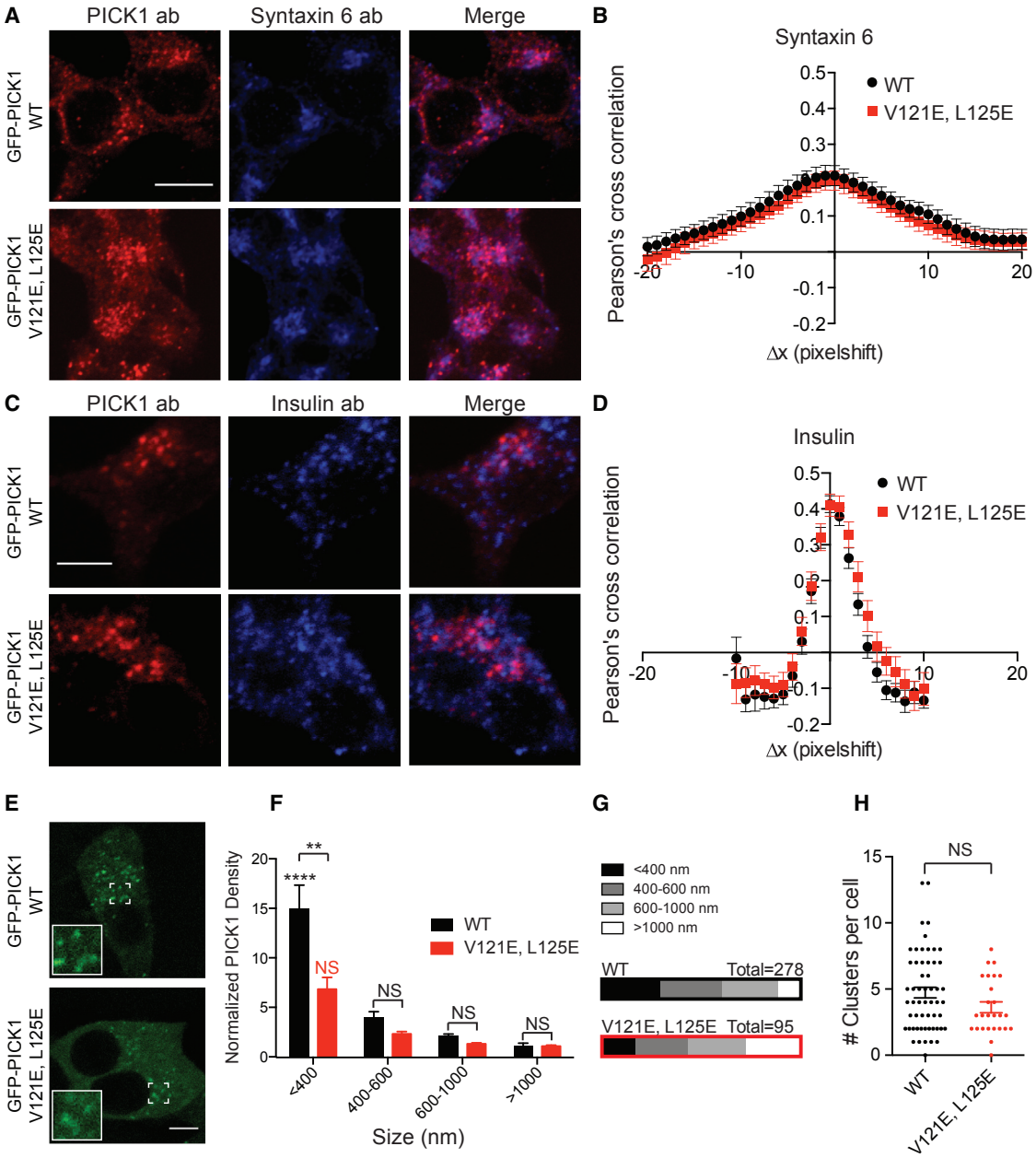

Figure 4. Disruption of the AH in PICK1 Alters the Cluster Distribution of PICK1 in INS1E Cells

(A and C) Representative confocal images of INS-1E cells transduced with lentiviral vectors knocking down endogenous PICK1 and encoding GFP-PICK1 (top) or GFP-PICK1 V121E, L125E (bottom). Images show immunosignal for PICK1 (red) and syntaxin 6 in (A) and insulin (blue) in (C) and the merged signals. Scale bars, 10 μM.(B and D) Quantification of colocalization between GFP-PICK1 (black) or GFP-PICK1 V121E, L125E (red) and syntaxin 6 in (B) (means ± SEM; ns = 44 and 42, respectively) and insulin in (D) (means ± SEM; ns = 68 and 47 cells, respectively) using Van Steensel's cross-correlation analysis that reports the Pearson cross-correlation as a function of the relative movement of the two channels with respect to each other (Δx). (3 independent experiments).

(E) Representative confocal images of live INS-1E cells, transduced with lentiviral vectors encoding PICK1 silencing shRNA (sh18) together with a shRNA-resistant rescue construct, GFP-PICK1 (top) or GFP-PICK1 V121E, L125E (bottom). Scale bar, 5 μM. Insets: close-ups of PICK1 containing punctae (250%).

(F) Density of fluorescence for clusters of different diameters for GFP-PICK1 (black) and GFP-PICK1 V121E, L125E (red). Data are means ± SEM for punctae identified by automated Gaussian fitting of fluorescence intensity across 56 and 26 cells for GFP-PICK1 and GFP-PICK1 V121E, L125E, respectively, (4 independent experiments). Density of GFP-PICK1—but not GFP-PICK1 V121E, L125E (diameters < 400 nm)—was significantly higher on small punctae than for other bins (**p < 0.01; ****p < 0.0001, two-way ANOVA, Newman-Keuls multiple comparisons test; NS, not significant).

(legend continued on next page)

GFP-PICK1 signal partially overlapped with that of the late Golgi/early secretory vesicle marker syntaxin 6 (Figure 4A), as supported by van Steensel's cross-correlation analysis (Figure 4B). In addition, we confirmed extensive overlap with insulin (Figures 4C, 4D) (Cao et al., 2013), together suggesting that GFP-PICK1 localizes, at least in part, to late Golgi and insulin-containing granules in INS-1E cells (Figures 4A–4D). Notably, GFP-PICK1 V121E, L125E did not localize differently from GFP-PICK1 (Figures 4A–4D).

To address putative curvature-sensitive cellular localization of GFP-PICK1 in live INS-1E cells (Figure 4E), we performed an automated detection based on Gaussian fitting of the GFP-PICK1 intensities. The results were binned according to the width of the Gaussian fit of the structure and, thus, their approximate size. Interestingly, we observed significantly higher density (see Experimental Procedures) of GFP-PICK1 on the small punctae (<400 nm) than on punctae of larger diameters (Figure 4F). GFP-PICK1 V121E, L125E displayed, overall, a similar type of punctate localization, but the structures appeared more diffuse (Figure 4A). Quantification of the punctae revealed some size dependence of the protein density but not significantly higher density on small punctae (<400 nm), compared to larger punctae. Moreover, the density of the small GFP-PICK1 WT punctae (<400 nm) was significantly higher than that of the small GFP-PICK1 V121E, L125E punctae (Figure 4F).

Evaluating the size distribution of GFP-PICK1 WT versus GFP-PICK1 V121E, L125E punctae revealed redistribution toward large punctae (>1,000 nm) at the expense of small punctae (<400 nm) for the mutant (Figure 4G). However, the average number of punctae identified per cell was not significantly different between GFP-PICK1 WT and GFP-PICK1 V121E, L125E (Figure 4H). Altogether, the data are consistent with the MCS capacity of the AH in PICK1 being critical for its high density on smaller vesicular structures, as predicted by *in vitro* liposome binding. These findings were, in essence, recapitulated by heterologous expression of YFP-PICK1 in COS7 cells (Figure S6).

The AH Directs Curvature-Sensitive Localization to Insulin Granules in INS-1E Cells

To directly investigate curvature-sensitive recruitment of PICK1 to insulin-containing granules, we turned to dual-color STORM (dSTORM). The insulin signal revealed multiple clusters of dense signal, presumably representing insulin granules. Both the GFP-PICK1 WT and mutant signals were present in clusters, of which a fair number overlapped with those of insulin (Figures 5A–5D). Cross-section through a single granule further demonstrated how the GFP-PICK1 signal localized to the periphery of the insulin granules (Figure 5E). Using only the high-precision data (see the Supplemental Experimental Procedures), we next used the insulin signal to outline the size of the granules, which ranged from 50 to 250 nm in GFP-PICK1-expressing cells, which is in good agreement with previous findings by electron microscopy (EM) from INS-1 cells (MacDonald et al., 2005). GFP-PICK1 V121E, L125E-expressing cells showed an almost identical size distribution of insulin granules, suggesting the PICK1 AH is not important for determining size of insulin granules (Figure 5F, left). For insulin granules colocalizing with GFP-PICK1, we next quantified how much GFP-PICK1 was contained on the structure (Figure S7). Both GFP-PICK1 WT and GFP-PICK1 V121E, L125E localized to granules ranging from 100 to 250 nm (Figure 5F, right) and with a distinct shift to larger sizes compared to the size distribution of the total granula population.

Importantly, the density of the GFP-PICK1 WT signal increased on granules of smaller size, whereas this pattern was less prominent for GFP-PICK1 V121E, L125E (Figure 5G). Indeed, quantification of the average density of granules above and below 145 nm in diameter demonstrated a significantly increased density of GFP-PICK1 on small liposomes, which was not the case for GFP-PICK1 V121E, L125E. Representative 3D-STORM images of single granules with GFP-PICK1 (shown as black open circles in Figure 5G) further highlight this selective difference in binding density on the smaller structures (Figure 5I). In summary, we find that the *in vitro* MCS capacity for PICK1 is also observed for PICK1 on insulin-containing granules and that the increased density on small structures (<150 nm) is dependent on the AH.

MCS by PICK1 Is Critical for Insulin Storage in INS-1E Cells

Insulin storage in, and secretion from, the pancreas of PICK1-deficient mice was recently demonstrated to be compromised, but whether this was a cell-autonomous effect is unknown (Cao et al., 2013; Holst et al., 2013). Therefore, we knocked down PICK1 expression using the lentivirally encoded shRNA (sh18 GFP) in INS-1E cells using GFP without shRNA as control (Figure 6A). In agreement with a role for PICK1 in insulin storage, quantification of individual experiments revealed a linear correlation (R^2 = 0.55) between PICK1 and the insulin immunosignal in control cells (GFP) (Figure 6B). Importantly, both the average PICK1 and the average insulin immunosignal were reduced in the shRNA-transduced cells, sh18 (mean), compared to control, GFP control (mean) (Figure 6B). To allow quantification across three independent experiments, the PICK1 and insulin immunosignals in the sh18 GFP- and control GFP-positive cells were normalized to the surrounding non-transduced cells. This demonstrated that the reduction of both the PICK1 and the insulin immunosignal was highly significant (Figures 6C and 6D). Note that, because of the low transduction efficiency of the INS-1E cells, it was not possible to reliably assess changes in insulin secretion, e.g., by ELISA; however, previous results support a strong connection between PICK1 depletion and compromised release (Cao et al., 2013; Holst et al., 2013).

To probe the functional role of the AH in this process, we first tested whether replacement of endogenous PICK1 with

(G) Size distribution of punctae for GFP-PICK1 (black) and GFP-PICK1 V121E, L125E (red). GFP-PICK1 V121E, L125E shows a significant shift in distribution from small (<400 nm) to large (>1,000 nm) punctae, χ^2 = 10.82, df = 3, p = 0.013.

(H) Average number of identified punctae per cell for GFP-PICK1 (black) and GFP-PICK1 V121E, L125E (red) was not significantly different (p = 0.094, unpaired t test). NS, not significant.

See also Figure S6.

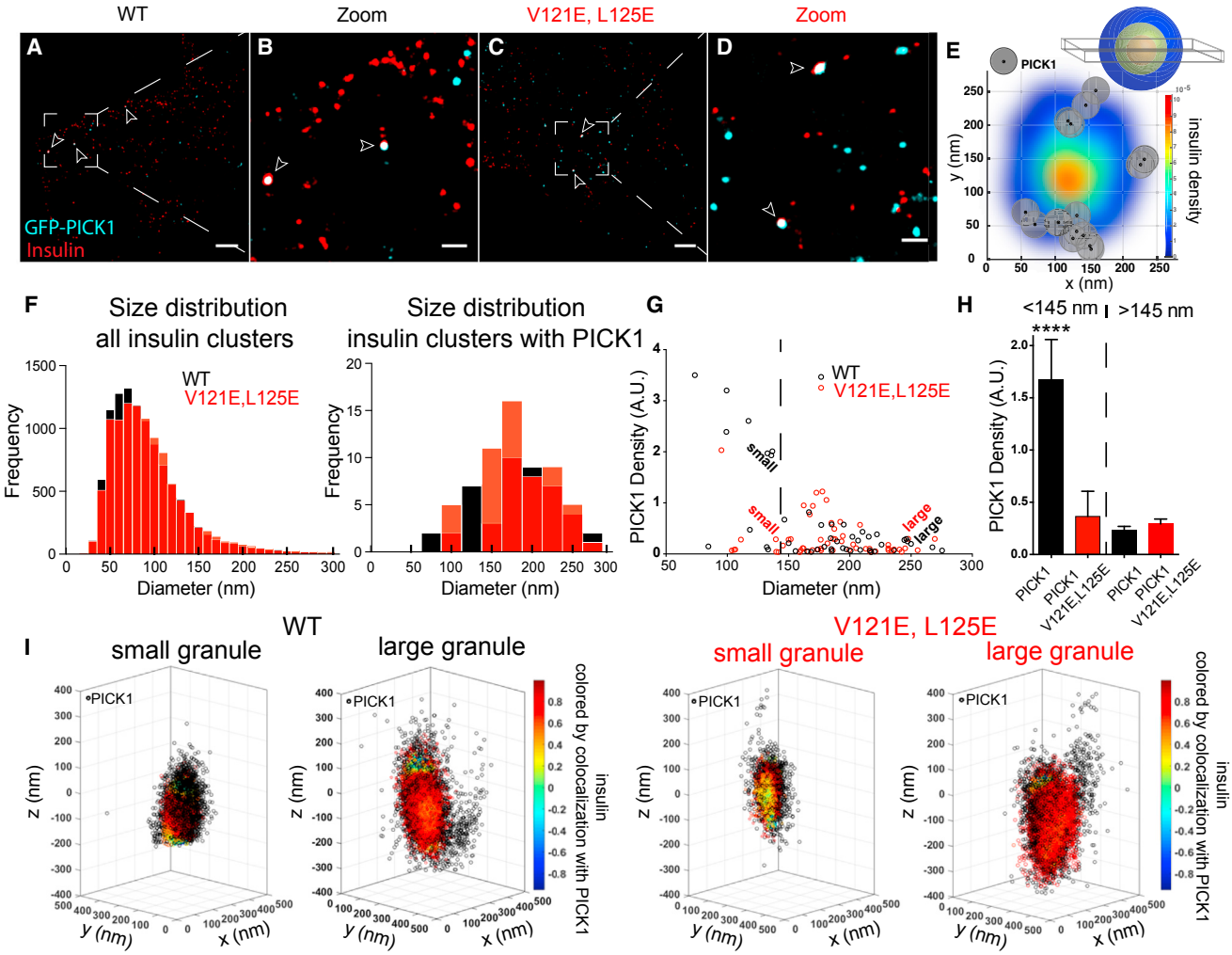

Figure 5. Disruption of the AH Alters the Distribution of PICK1 in INS1E Cells

(A–D) Representative dSTORM images of INS1-E cells transduced with lentiviral vectors encoding GFP-PICK1 (top) (A and zoom in B [400%]) or GFP-PICK1 V121E, L125E (C and zoom in D [400%]). Images show immunosignal for GFP-PICK1 (CF568, cyan) and insulin (Alexa Fluor 647, red). Only points localized with precision better than 20 nm are shown, and colocalizations are indicated with open arrowheads. Scale bars, 2 μM; 500 nm in zooms.

(E) Cross-section (100 nm) of a single insulin granule (color coded by insulin density). The PICK1 signal is shown as localization center (black) and localization precision (gray circle) and is localized around the periphery of the granule.

(F) Left: size of insulin granules in GFP-PICK1- (black) and GFP-PICK1 V121E, L125E (red)-expressing INS1-E cells. Right: size of insulin granules colocalized with PICK1 GFP-PICK1 (black) and GFP-PICK1 V121E, L125E (red).

(G) Density of GFP-PICK1 (black) and GFP-PICK1 V121E, L125E (red) on individual insulin clusters of different size (as determined by the x-y plane). Pooled from three experiments.

(H) Quantification of average density of GFP-PICK1 (black) and GFP-PICK1 V121E, L125E (red) on individual insulin cluster below and above 145 nm from (G). GFP-PICK1 density on granules below 145 nm was significantly higher than that on granules above 145 nm and that of GFP-PICK1 V121E, L125E in both categories (all ps < 0.0001, two-way ANOVA, followed by Tukey's multiple comparisons test). ****p < 0.0001. Data are means ± SEM.

(G and H) The dotted line at 145 nm indicates separation of small and large granules used for quantification in H.

(I) Examples (indicated in G) of GFP-PICK1 (left) and GFP-PICK1 V121E, L125E (right) localized in each case to a single small and a single large insulin-containing granule resolved by 3D-STORM. PICK1 is indicated in black, and insulin is color coded by colocalization with PICK1.

See also Figure S7.

shRNA-resistant GFP-PICK1 could rescue the reduced insulin levels (Figure 6E). We quantified the PICK1 and the insulin immunosignal in GFP-PICK1-expressing cells and found a linear correlation between the insulin and the PICK1 signal, indicative of rescue (Figure 6F). Note that the average mean intensity of the signals upon shRNA-mediated knockdown of PICK1 (no rescue) was used as an offset for the correlation (hexagon symbol in Figure 6F). Importantly, replacement with shRNA-resistant GFP-PICK1 V121E, L125E was less efficient than GFP-PICK1 (indicated by a shallower slope; Figures 6F and 6G). This supports a role of PICK1 in maintaining insulin levels in INS-1E cells that depends on the MCS capacity conferred by the AH.

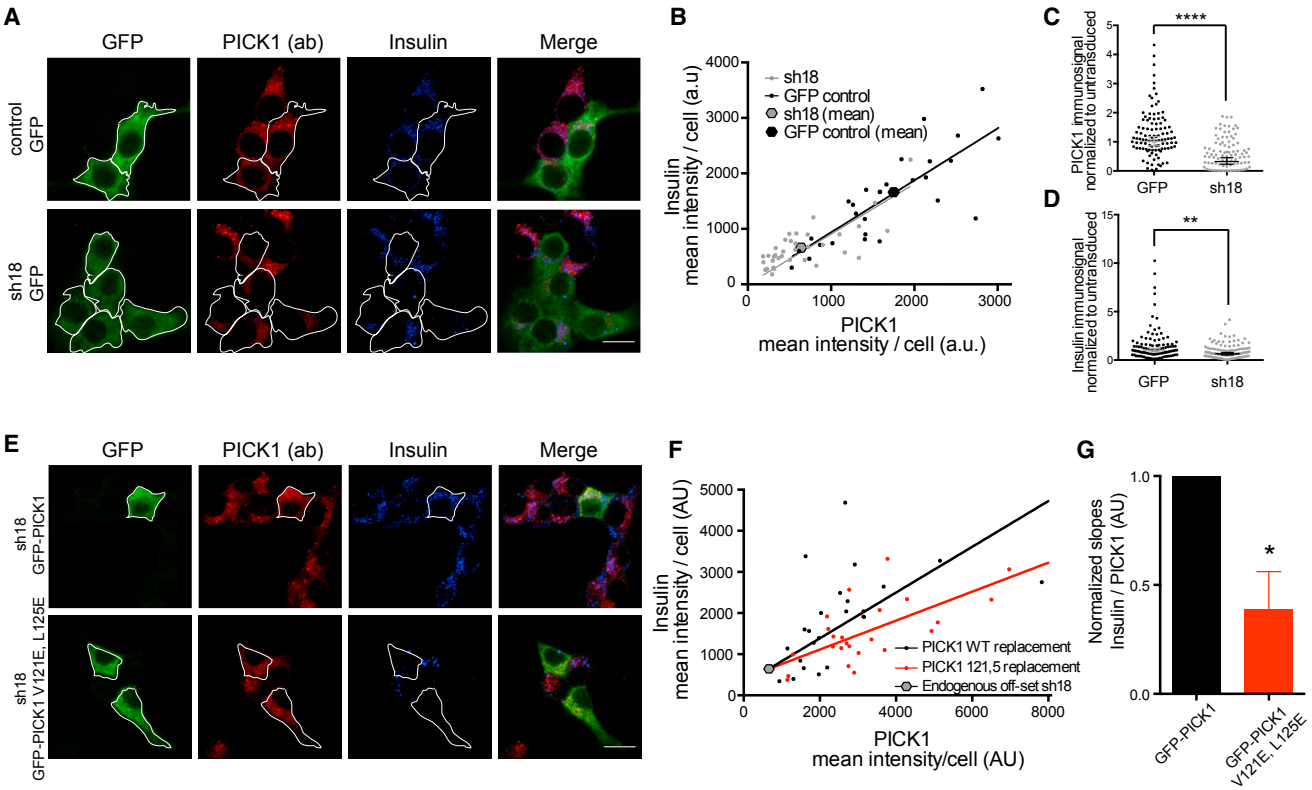

Figure 6. Disruption of the AH in PICK1 Reduces Insulin Content in INS-1E Cells

(A) Representative confocal images of INS-1E cells transduced with lentiviral vectors encoding GFP (top) or GFP and shRNA silencing PICK1 (sh18, bottom). Images show GFP control (green), PICK1 (red), and insulin (blue), as well as a merge of the three images. Scale bar, 10 μM.

(B) Plot of PICK1 versus insulin immunosignal from a single experiment (out of three) showing a linear relationship ($R^2 = 0.55$). Average intensities (hexagons) show reduction of both PICK1 and insulin signals in cells with PICK1 knockdown (KD) (sh18).

(C and D) PICK1 (C) or insulin (D) immunosignal with (sh18) or without (GFP) lentiviral PICK1 KD in INS-1E cells, normalized to levels of non-transduced cells in the same image. Each dot represents a single cell. Both the PICK1 and the insulin signal were significantly reduced upon PICK1 KD. **$p < 0.01$; ****$p < 0.0001$, unpaired t test with Welch correction; ns = 104 (GFP) and 90 (sh18) individual cells, 3 independent experiments.

(E) Representative confocal images of INS-1E cells, transduced with lentiviral vectors encoding the PICK1 shRNA (sh18) together with shRNA-resistant rescue construct GFP-PICK1 (top panels) or GFP-PICK1 V121E, L125E (bottom panels). Images show GFP control (green), PICK1 (red), and insulin (blue), as well as a merge of the three images. Scale bar, 10 μM.

(F) Plot of PICK1 versus insulin immunosignal from a single experiment (out of three) in INS-1E cells rescued with WT GFP-PICK1 (black symbols) or GFP-PICK1 V121E, L125E (red symbols).

(G) Quantification of normalized slopes from (F) (means ± SEM, n = 3). *$p < 0.05$, unpaired t test with Welch correction.

The AH Is Critical for the Function of *Drosophila* PICK1 in Metabolic Regulation

Previously, we reported that *Drosophila* PICK1 (dPICK1) is widely expressed in the neuroendocrine system (Jansen et al., 2009) and that *dPICK1* null mutant flies suffer from a significant weight loss that is likely related to dysfunction of peptide-secreting cells regulating fly metabolism (Holst et al., 2013). Alignment and helical wheel projection strongly indicate that an AH is also present in dPICK1 and that the helix-disrupting mutations correspond to L123E and I127E (indicated with asterisks and arrows in Figures 7A and 7B, respectively). These mutations were introduced into a transgenic WT rescue construct also carrying a hemagglutinin tag (*dPICK1-HA*). Both the mutant transgene (*dPICK1-HA L123E, I127E*) and *dPICK1-HA* were targeted for insertion to the same site in the genome using PhiC31 recombination, ensuring identical expression levels (Figure 7C).

We expressed *dPICK1-HA* in a dPICK1 mutant background under the *dimm* promoter specific for large neuropeptidergic cells (Park et al., 2008) and examined neuropeptidergic cell bodies in the pupal ventral nerve cord, the caudal region of the *Drosophila* CNS. In peptidergic cell bodies, the *dPICK1-HA* immunosignal formed punctae closely associated with GFP-tagged Golgin 245, a *trans*-Golgi marker (Sinka et al., 2008) (Figures 7D and 7E). In contrast, in flies expressing *dPICK1-HA L123E, I127E*, the immunosignal was generally more diffuse, although some association with the *trans*-Golgi marker was detected (Figures 7D and 7E).

We had observed earlier that a WT *dPICK1* transgene can rescue the weight loss of *dPICK1* null mutant flies (Holst et al., 2013). Strikingly, when expressed under the control of the pan-peptidergic prohormone convertase 2 promoter, only the *dPICK1-HA* transgene was able to rescue the weight deficit,

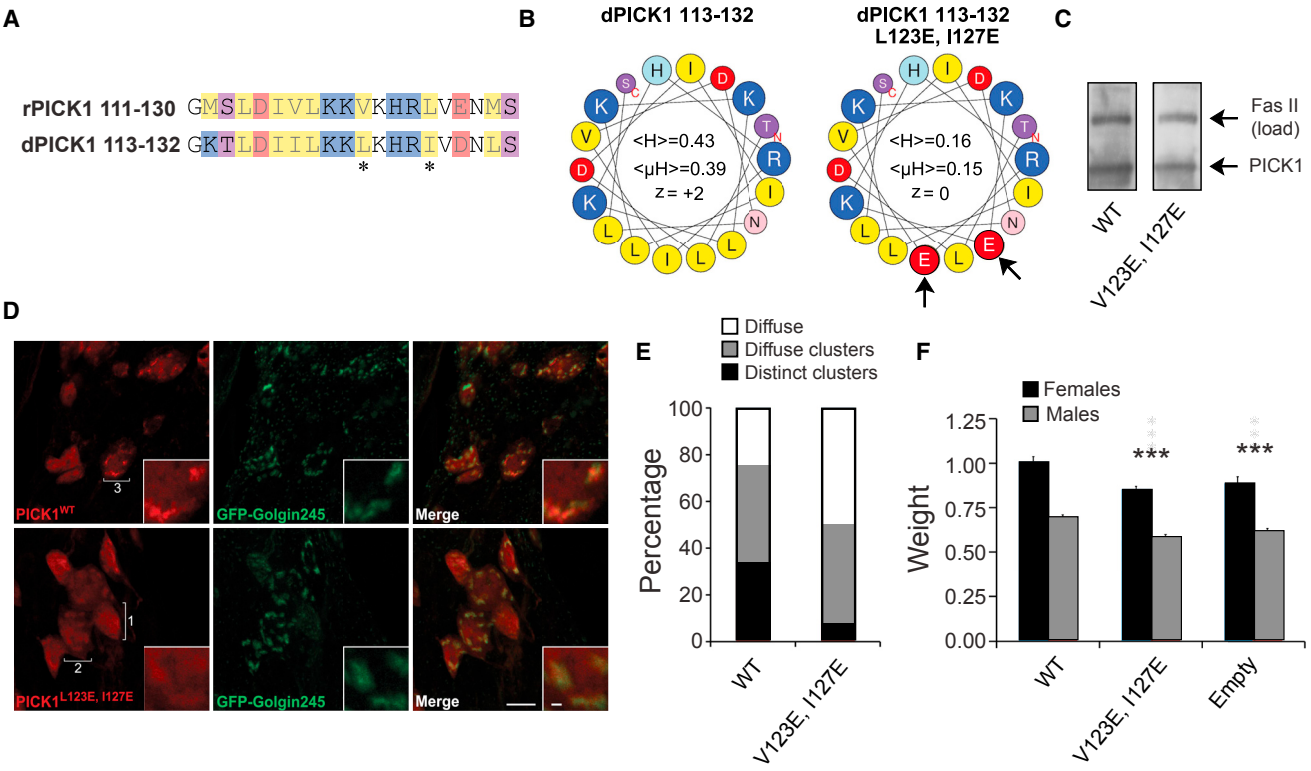

Figure 7. Disruption of the AH in dPICK1 Compromises Localization and Physiological Function of PICK1 in Endocrine Cells of Fruit Flies

(A) Sequence alignment of the AH preceding the BAR domain in rat and *Drosophila* PICK1. Asterisks indicate helix-disrupting mutations.

(B) Helical wheel projections of the AH in dPICK WT (left) and dPICK L123E and I127E (right, indicated by arrows).

(C) Immunoblot of dPICK1-HA or *dPICK-HA L123E, I127E* transgene in *dPICK1* null flies, controlled by the prohormone convertase 2 promoter specific for peptidergic cells.

(D) Representative confocal images showing immunohistochemical labeling of WT (top) and dPICK1-HA L123E, I127E (bottom) expressed in the ventral nerve cord of *dPICK1* null pupal flies under the control of the peptidergic *dimm* promoter. The cells also expressed the *trans*-Golgi network marker GFP-Golgin245. Scale bars, 10 μm; 1 μm in inset.

(E) Quantification of the cellular distribution of dPICK1-HA and dPICK1-HA L123E, I127E in (D). Cells were classified according to the distribution pattern of the dPICK1-HA immunosignal: diffuse distribution, diffuse aggregates broadly coinciding with Golgi complexes, or distinct aggregates coinciding with or surrounding Golgi complexes. WT dPICK1-HA: six individuals, 252 cells. dPICK1-HA L123E, I127E: four individuals, 140 cells. The distribution patterns differed significantly, $\chi^2 = 43.2$, df = 2, $p < 0.0001$.

(F) Body weight of adult flies expressing WT *dPICK-HA*; dPICK1-HA L123E, I127E; or no transgene in a *dPICK1* null background. ***$p < 0.0005$, compared to WT (two-way ANOVA, followed by Tukey test).

while *dPICK1-HA L123E, I127E* was not (Figure 7F). These findings support a critical role for the AH in the function of dPICK1 in metabolic regulation.

DISCUSSION

Selective membrane binding is crucial for the function of numerous cytosolic proteins, including kinases, GTPases, scaffolding proteins, and proteins involved in reshaping the membrane. Here, we identify an amphipathic helix as a membrane-binding motif in the IPA BAR proteins, including ICA69, PICK1, and arfaptin. We find that, similar to bona fide N-BAR proteins like endophilin (Bhatia et al., 2009), the IPA BAR proteins display robust membrane binding that is sensitive to spherical curvature. Similar helices were identified recently in the sorting nexin family of BAR domain proteins, categorizing them as N-BAR proteins as well (van Weering et al., 2012). This suggests a wide distribution of the N-BAR protein properties among all of the proteins belonging to the regular BAR domain family (excluding I-BARs and F-BARs).

The presence of AHs in IPA BAR proteins is not surprising from an evolutionary point of view and has previously been hinted at in the literature. In the seminal paper by McMahon and co-workers, which defined the BAR domain as a functional entity, it was demonstrated that the N-terminal part of arfaptin 2, rather than the BAR domain itself, was responsible for the majority of membrane binding, but the reason for this was not identified (Peter et al., 2004). Recently, AHs were suggested to precede the BAR domain in the arfaptins and mutation of a conserved tryptophan in the predicted hydrophobic wedge reduced *in vitro* membrane binding (Cruz-Garcia et al., 2013). For PICK1, we demonstrated that the mutations used in the present study abolish the membrane-deforming capacity *in vitro* (Holst et al., 2013), but the effect on MCS was not elucidated.

Here, with super-resolution microscopy, we were able to resolve the actual size of insulin-containing granules in endocrine INS-1E cells and confirm AH-dependent MCS in a cellular environment. We suggest that PICK1 localizes to immature granules at increasing density, as the granules condense before leaving the final mature structures—perhaps by being directly involved with the selective removal of excess membrane material during maturation.

Both in endophilin and in amphiphysin, the functional importance of AHs was supported by cellular redistribution of the proteins from their respective lipid compartment to the cytosol upon truncation or mutation of the helices (Farsad et al., 2001; Takei et al., 1999). The arfaptins were likewise demonstrated to redistribute from the Golgi apparatus to the cytosol upon mutations in the AH (Cruz-Garcia et al., 2013), and endophilin mutated in the amphipathic helix failed to rescue the lethality of endophilin null fruit flies (Jung et al., 2010). Nonetheless, because AH mutations nearly eliminated lipid binding of these proteins (Bhatia et al., 2009), it was not possible to assess whether the functional effect was due to reduced overall lipid binding or compromised MCS. We observed similarly that for the PICK1 N-BAR domain (PICK1 Δ101), mutation of the helix (V121E, L125E) almost abolished membrane binding. In the full-length PICK1, however, the mutations in the AH (V121E, L125E) did not reduce overall liposome binding or vesicle association in cells but selectively perturbed MCS, thus enabling us to move past the functional significance of membrane binding per se. Of note, a mutation in the AH of the BAR domain protein BIN1, which was associated with autosomal recessive centronuclear myopathy, did also not reduce overall membrane binding, but the functional consequences of this mutation with respect to membrane curvature were not assessed (Wu and Baumgart, 2014).

From a conceptual standpoint, it is reassuring that the spherical MCS determined from the *in vitro* SLiC assay (Bhatia et al., 2009; Hatzakis et al., 2009) has biological implications in cells. The SLiC assay uses separate lipid compartments with little or no exchange of lipid material. The situation in cells is markedly different for two reasons. First, curved cellular membranes arise from continuous membranes that undergo deformation. Second, lipid material is transferred between lipid compartments *in vivo*. It was, therefore, of general importance to correlate MCS measured *in vitro* with protein distribution in live cells. Remarkably, we showed that the helix-disrupting mutation entails markedly impaired MCS ability in the SLiC assay, as well as significant redistribution of protein away from small insulin granules in live cells. We conclude, accordingly, that spherical MCS, as assessed in the SLiC assay as well as in equivalent cell-based assays, represents a key aspect of membrane-binding specificity in BAR domain proteins, with direct implications for cellular localization and physiological function.

In summary, we demonstrate the presence of a functionally indispensable AH located N-terminal to the BAR domain in the IPA group of BAR domain proteins encompassing arfaptins 1 and 2, ICA69, and PICK1. Importantly, we substantiate our biochemical and biophysical data for PICK1 with functional experiments in endocrine cells as well as *in vivo* in a *Drosophila* model. Our findings highlight MCS as an important biological mechanism for establishing membrane-binding specificity in cells, not only for N-BAR proteins but likely also for other proteins carrying membrane-binding AHs.

EXPERIMENTAL PROCEDURES

Molecular Biology

Plasmids for expression and purification of PICK1, arfaptin 2, and ICA69 constructs were described previously (Madsen et al., 2005) or generated as described in the Supplemental Experimental Procedures. Arfaptin 2 in the pGEX 6P1 GST vector was a gift from Dr. Harvey T. McMahon (MRC Laboratory of Molecular Biology, Cambridge, UK). FUGW shPICK1 GFP and FUGW shPICK1 GFPPICK1 constructs were provided by Robert Malenka, Stanford, CA, USA. The GFP control vector was generated by deleting the shRNA. Mutations were introduced by Quick Change.

Protein Purification

PICK1 and arfaptin 2, as well as truncated AHs, were expressed as GST fusion proteins in the *E. coli* BL21 DE3 and purified as described previously (Madsen et al., 2005). ICA69 fused to maltose binding protein (MBP) was expressed in *E. coli* BL21 DE3, purified using amylose resin. Proteins were fluorescently labeled with Alexa 488 C5 maleimide. See also the Supplemental Experimental Procedures.

SLiC Assay

The SLiC assay (Bhatia et al., 2009; Hatzakis et al., 2009) was performed as described in the Supplemental Experimental Procedures.

Computational Methods

The computational methods are described in the Supplemental Experimental Procedures.

INS-1E Cells

Cell culture, transduction, immunocytochemistry, and imaging are described in a supplemental modified one-channel version of the SLiC routine in Igor Pro 6.3 (Bhatia et al., 2009; Hatzakis et al., 2009). Initial inclusion criteria for cluster selection (minimum area, image threshold, and maximum deviation of Gaussian fits) were evaluated by visual inspection and kept fixed throughout the analysis. Further cluster selection was done by 3D-Gaussian fitting of the point-spread function of the punctae. Quantification was done by extracting single-particle positions and using background-corrected integrated fluorescence intensities for all punctae. Densities were calculated as the integrated fluorescence intensity divided by the area given by the Gaussian fit. Diameters were calculated from the Gaussian fit area assuming circular structures. For details, see the Supplemental Experimental Procedures.

3D STORM

INS-1E cells transduced with GFP-PICK1 WT or mutant were permeabilized and immunolabeled with primary antibodies to GFP and insulin and secondary antibodies conjugated with either Alexa Fluor 647 (insulin) or CF568 (GFP). Localizations were collected through the software ThunderSTORM, and points with uncertainty < 20.0 nm were selected. 3D images were acquired through optical astigmatism and calibrated on samples of immobilized fluorescent beads taken at each imaging session (see also the Supplemental Experimental Procedures. Coordinate-based colocalization (CBC) of PICK1/insulin cluster analysis was done through home-written Python and MATLAB scripts and described in the Supplemental Experimental Procedures and Figure S7. Custom written codes are available at: https://github.com/GetherLab/Super-Resolution-Data-Analysis.

Drosophila

HA-tagged transgenes encoding WT PICK1 and PICK1 L123E, I127E were inserted into the M{3xP3-RFP.attP}ZH-86Fb attP site on the third chromosome using Phi31C transformation. The *UAS-EGFP-Golgin245* transgene was transformed into w^{1118} flies using standard P-element transformation. $PICK1^{1}$ and $PICK1^{2}$ null alleles have been described previously (Holst et al., 2013; Jansen et al., 2009). The *c929-GAL4* driver line was a gift from Dr. P. Taghert,

Washington University, St. Louis, MO, USA. The pan-peptidergic *386Y-GAL4* driver line was obtained from the Bloomington Drosophila Stock Collection (stock #25410). The body weight assay was done as described previously (Holst et al., 2013). See also Supplemental Experimental Procedures.

Statistics

Data are presented as individual liposomes, individual cells, or averages ± SEM from three independent experiments. Direct comparisons were done by one- or two-way ANOVA followed by appropriate post-test. Distributions were compared using the chi-square test. Errors in MD were estimated using Monte Carlo bootstrapping. *$p < 0.05$; **$p < 0.01$; ***$p < 0.001$; and ****$p < 0.0001$.

SUPPLEMENTAL INFORMATION

Supplemental Information includes Supplemental Experimental Procedures and seven figures and can be found with this article online at https://doi.org/10.1016/j.celrep.2018.04.074.

ACKNOWLEDGMENTS

We thank Nabeela Khadim for technical assistance. The work was supported by NIH grants R01 DA 12408 (to U.G. and H.W.) and U54 GM087519 (to H.W.), the Danish Council for Independent Research – Medical Sciences (0602-02369B and 6110-00625B to U.G. and K.L.M.), the Lundbeck Foundation Center for Biomembranes in Nanomedicine (2009-4585 to U.G. and D.S.), the UNIK Center for Synthetic Biology (to U.G., K.L.M., and D.S.), the Lundbeck Foundation (2012-10634 to O.K.), the Brødrene Hartmanns Foundation (to O.K.), the Novo Nordisk Foundation (NNF14OC0012733 and NNF12OC0002181 to U.G.), and the 1923 Fund (to H.W. and G.K.). The use of computational resources of the David A. Cofrin Center for Biomedical Information in the Institute for Computational Biomedicine at Weill Cornell Medical College is gratefully acknowledged.

AUTHOR CONTRIBUTIONS

K.L.M., R.H., R.C.A., I.A.-J., V.K.L., T.S.P., M.S., N.R.C., S.E., and V.B. conducted in vitro and COS-7 cell experiments with help from J.B.L. A.M.J., M.D.L., and R.C.A. conducted INS-1E and 3D-STORM experiments. V.K.L. and O.K. conducted *Drosophila* experiments. K.L.M., R.H., M.D.L., R.C.A., A.M.J., V.K.L., S.E., J.B.L., O.K., and U.G. analyzed data. G.K., N.J., P.B.C.A., and H.W. conducted MD simulations. K.L.M., R.H., A.M.J., V.K.L., G.K., N.J., H.W., O.K., D.S., and U.G. designed the experiments. K.L.M., R.H., O.K., G.K., N.J., H.W., D.S., and U.G. participated in writing the manuscript.

DECLARATION OF INTERESTS

The authors declare no competing interests.

Received: February 1, 2017
Revised: March 5, 2018
Accepted: April 17, 2018
Published: May 15, 2018

REFERENCES

Bhatia, V.K., Madsen, K.L., Bolinger, P.Y., Kunding, A., Hedegård, P., Gether, U., and Stamou, D. (2009). Amphipathic motifs in BAR domains are essential for membrane curvature sensing. EMBO J. *28*, 3303–3314.

Cao, M., Mao, Z., Kam, C., Xiao, N., Cao, X., Shen, C., Cheng, K.K., Xu, A., Lee, K.M., Jiang, L., and Xia, J. (2013). PICK1 and ICA69 control insulin granule trafficking and their deficiencies lead to impaired glucose tolerance. PLoS Biol. *11*, e1001541.

Chen, M., Cuendet, M.A., and Tuckerman, M.E. (2012). Heating and flooding: a unified approach for rapid generation of free energy surfaces. J. Chem. Phys. *137*, 024102.

Citri, A., Bhattacharyya, S., Ma, C., Morishita, W., Fang, S., Rizo, J., and Malenka, R.C. (2010). Calcium binding to PICK1 is essential for the intracellular retention of AMPA receptors underlying long-term depression. J. Neurosci. *30*, 16437–16452.

Cruz-Garcia, D., Ortega-Bellido, M., Scarpa, M., Villeneuve, J., Jovic, M., Porzner, M., Balla, T., Seufferlein, T., and Malhotra, V. (2013). Recruitment of arfaptins to the trans-Golgi network by PI(4)P and their involvement in cargo export. EMBO J. *32*, 1717–1729.

Cui, H., Lyman, E., and Voth, G.A. (2011). Mechanism of membrane curvature sensing by amphipathic helix containing proteins. Biophys. J. *100*, 1271–1279.

Doherty, G.J., and McMahon, H.T. (2009). Mechanisms of endocytosis. Annu. Rev. Biochem. *78*, 857–902.

Drin, G., and Antonny, B. (2010). Amphipathic helices and membrane curvature. FEBS Lett. *584*, 1840–1847.

Farsad, K., Ringstad, N., Takei, K., Floyd, S.R., Rose, K., and De Camilli, P. (2001). Generation of high curvature membranes mediated by direct endophilin bilayer interactions. J. Cell Biol. *155*, 193–200.

Galic, M., Jeong, S., Tsai, F.C., Joubert, L.M., Wu, Y.I., Hahn, K.M., Cui, Y., and Meyer, T. (2012). External push and internal pull forces recruit curvature-sensing N-BAR domain proteins to the plasma membrane. Nat. Cell Biol. *14*, 874–881.

Gallop, J.L., and McMahon, H.T. (2005). BAR domains and membrane curvature: bringing your curves to the BAR. Biochem. Soc. Symp. (*72*), 223–231.

Gautier, R., Douguet, D., Antonny, B., and Drin, G. (2008). HELIQUEST: a web server to screen sequences with specific α-helical properties. Bioinformatics *24*, 2101–2102.

Gehart, H., Goginashvili, A., Beck, R., Morvan, J., Erbs, E., Formentini, I., De Matteis, M.A., Schwab, Y., Wieland, F.T., and Ricci, R. (2012). The BAR domain protein arfaptin-1 controls secretory granule biogenesis at the trans-Golgi network. Dev. Cell *23*, 756–768.

Hanley, J.G. (2008). PICK1: a multi-talented modulator of AMPA receptor trafficking. Pharmacol. Ther. *118*, 152–160.

Hatzakis, N.S., Bhatia, V.K., Larsen, J., Madsen, K.L., Bolinger, P.Y., Kunding, A.H., Castillo, J., Gether, U., Hedegård, P., and Stamou, D. (2009). How curved membranes recruit amphipathic helices and protein anchoring motifs. Nat. Chem. Biol. *5*, 835–841.

Hess, B., Kutzner, C., van der Spoel, D., and Lindahl, E. (2008). GROMACS 4: algorithms for highly efficient, load-balanced, and scalable molecular simulation. J. Chem. Theory Comput. *4*, 435–447.

Holst, B., Madsen, K.L., Jansen, A.M., Jin, C., Rickhag, M., Lund, V.K., Jensen, M., Bhatia, V., Sørensen, G., Madsen, A.N., et al. (2013). PICK1 deficiency impairs secretory vesicle biogenesis and leads to growth retardation and decreased glucose tolerance. PLoS Biol. *11*, e1001542.

Hsieh, W.T., Hsu, C.J., Capraro, B.R., Wu, T., Chen, C.M., Yang, S., and Baumgart, T. (2012). Curvature sorting of peripheral proteins on solid-supported wavy membranes. Langmuir *28*, 12838–12843.

Iversen, L., Mathiasen, S., Larsen, J.B., and Stamou, D. (2015). Membrane curvature bends the laws of physics and chemistry. Nat. Chem. Biol. *11*, 822–825.

Jansen, A.M., Nässel, D.R., Madsen, K.L., Jung, A.G., Gether, U., and Kjaerulff, O. (2009). PICK1 expression in the Drosophila central nervous system primarily occurs in the neuroendocrine system. J. Comp. Neurol. *517*, 313–332.

Jin, W., Ge, W.P., Xu, J., Cao, M., Peng, L., Yung, W., Liao, D., Duan, S., Zhang, M., and Xia, J. (2006). Lipid binding regulates synaptic targeting of PICK1, AMPA receptor trafficking, and synaptic plasticity. J. Neurosci. *26*, 2380–2390.

Jung, A.G., Labarrera, C., Jansen, A.M., Qvortrup, K., Wild, K., and Kjaerulff, O. (2010). A mutational analysis of the endophilin-A N-BAR domain performed in living flies. PLoS ONE *5*, e9492.

Larsen, J.B., Jensen, M.B., Bhatia, V.K., Pedersen, S.L., Bjørnholm, T., Iversen, L., Uline, M., Szleifer, I., Jensen, K.J., Hatzakis, N.S., and Stamou, D. (2015). Membrane curvature enables N-Ras lipid anchor sorting to liquid-ordered membrane phases. Nat. Chem. Biol. *11*, 192–194.

Lu, W., and Ziff, E.B. (2005). PICK1 interacts with ABP/GRIP to regulate AMPA receptor trafficking. Neuron *47*, 407–421.

MacDonald, P.E., Obermüller, S., Vikman, J., Galvanovskis, J., Rorsman, P., and Eliasson, L. (2005). Regulated exocytosis and kiss-and-run of synaptic-like microvesicles in INS-1 and primary rat beta-cells. Diabetes *54*, 736–743.

Madsen, K.L., Beuming, T., Niv, M.Y., Chang, C.W., Dev, K.K., Weinstein, H., and Gether, U. (2005). Molecular determinants for the complex binding specificity of the PDZ domain in PICK1. J. Biol. Chem. *280*, 20539–20548.

Madsen, K.L., Eriksen, J., Milan-Lobo, L., Han, D.S., Niv, M.Y., Ammendrup-Johnsen, I., Henriksen, U., Bhatia, V.K., Stamou, D., Sitte, H.H., et al. (2008). Membrane localization is critical for activation of the PICK1 BAR domain. Traffic *9*, 1327–1343.

Madsen, K.L., Bhatia, V.K., Gether, U., and Stamou, D. (2010). BAR domains, amphipathic helices and membrane-anchored proteins use the same mechanism to sense membrane curvature. FEBS Lett. *584*, 1848–1855.

Marrink, S.J., Risselada, H.J., Yefimov, S., Tieleman, D.P., and de Vries, A.H. (2007). The MARTINI force field: coarse grained model for biomolecular simulations. J. Phys. Chem. B *111*, 7812–7824.

Mim, C., Cui, H., Gawronski-Salerno, J.A., Frost, A., Lyman, E., Voth, G.A., and Unger, V.M. (2012). Structural basis of membrane bending by the N-BAR protein endophilin. Cell *149*, 137–145.

Monticelli, L., Kandasamy, S.K., Periole, X., Larson, R.G., Tieleman, D.P., and Marrink, S.J. (2008). The MARTINI coarse-grained force field: extension to proteins. J. Chem. Theory Comput. *4*, 819–834.

Moravcevic, K., Oxley, C.L., and Lemmon, M.A. (2012). Conditional peripheral membrane proteins: facing up to limited specificity. Structure *20*, 15–27.

Nguyen, N., Shteyn, V., and Melia, T.J. (2017). Sensing membrane curvature in macroautophagy. J. Mol. Biol. *429*, 457–472.

Pan, L., Wu, H., Shen, C., Shi, Y., Jin, W., Xia, J., and Zhang, M. (2007). Clustering and synaptic targeting of PICK1 requires direct interaction between the PDZ domain and lipid membranes. EMBO J. *26*, 4576–4587.

Park, D., Veenstra, J.A., Park, J.H., and Taghert, P.H. (2008). Mapping peptidergic cells in *Drosophila*: where DIMM fits in. PLoS ONE *3*, e1896.

Peter, B.J., Kent, H.M., Mills, I.G., Vallis, Y., Butler, P.J., Evans, P.R., and McMahon, H.T. (2004). BAR domains as sensors of membrane curvature: the amphiphysin BAR structure. Science *303*, 495–499.

Poudel, K.R., Dong, Y., Yu, H., Su, A., Ho, T., Liu, Y., Schulten, K., and Bai, J. (2016). A time course of orchestrated endophilin action in sensing, bending, and stabilizing curved membranes. Mol. Biol. Cell *27*, 2119–2132.

Sinka, R., Gillingham, A.K., Kondylis, V., and Munro, S. (2008). Golgi coiled-coil proteins contain multiple binding sites for Rab family G proteins. J. Cell Biol. *183*, 607–615.

Sorre, B., Callan-Jones, A., Manzi, J., Goud, B., Prost, J., Bassereau, P., and Roux, A. (2012). Nature of curvature coupling of amphiphysin with membranes depends on its bound density. Proc. Natl. Acad. Sci. USA *109*, 173–178.

Takei, K., Slepnev, V.I., Haucke, V., and De Camilli, P. (1999). Functional partnership between amphiphysin and dynamin in clathrin-mediated endocytosis. Nat. Cell Biol. *1*, 33–39.

van Weering, J.R., Sessions, R.B., Traer, C.J., Kloer, D.P., Bhatia, V.K., Stamou, D., Carlsson, S.R., Hurley, J.H., and Cullen, P.J. (2012). Molecular basis for SNX-BAR-mediated assembly of distinct endosomal sorting tubules. EMBO J. *31*, 4466–4480.

Wu, T., and Baumgart, T. (2014). BIN1 membrane curvature sensing and generation show autoinhibition regulated by downstream ligands and PI(4,5)P2. Biochemistry *53*, 7297–7309.

Xu, J., and Xia, J. (2006-2007). Structure and function of PICK1. Neurosignals *15*, 190–201.